Growth of porous single-crystal Cr_2O_3 in a 3-D mesopore system

Kun Jiao,[a] Bin Zhang,[a] Bin Yue,[a] Yu Ren,[a] Shixi Liu,[a] Shirun Yan,[a] Calum Dickinson,[b] Wuzong Zhou*[b] and Heyong He*[a]

Received (in Cambridge, UK) 25th August 2005, Accepted 27th September 2005
First published as an Advance Article on the web 20th October 2005
DOI: 10.1039/b512080b

Single-crystal Cr_2O_3 with regular mesopores has been synthesized using mesoporous silica KIT-6 as a template and characterized by using XRD, HRTEM and nitrogen adsorption/desorption.

Synthesis of ordered mesoporous silicas has attracted much attention due to their potential applications in the fields of catalysis, functional materials, and nanodevices.[1–5] Many mesoporous siliceous materials, such as MCM-48, MCM-41, SBA-15 and KIT-6, have been prepared by the self-assembly method using long-chain surfactants as templates over the past decade.[6–9] Non-siliceous mesoporous materials, especially transition-metal oxides, can also be prepared in a similar way, so-called soft chemical templating route, with some difficulties arising due to the low structural stability of the mesoporous intermediates containing both transition metal oxides and surfactants.[10] All of these materials have amorphous walls. For chromium oxide, Rao and co-workers synthesized a mesostructured lamellar phase using the soft templating method.[11] The chromium oxide layers are non-crystalline and contain mixed cations of Cr^{6+} and Cr^{3+}. Another method, using hard templates to nanocast non-siliceous materials, has also been developed in the recent years. Various templates, such as porous anodic aluminium oxides, mesoporous silicas or carbon nanotubes, can be used as nanoscale reactors for preparing one-dimensional (1-D) nanorods or nanowires.[12–14] Furthermore, three-dimensional (3-D) replicas can be obtained when the templates with a 3-D porous framework are used.[15–17] However, the structures of most of these materials are either amorphous or polycrystalline. In our previous studies, we have fabricated porous single-crystal Cr_2O_3 and WO_3 using mesoporous silica SBA-15 as the template where the interconnected smaller mesopores and/or micropores among the main mesoporous channels help the growth of 3-D porous single-crystals of the transition metal oxides.[18,19] In the present work, we demonstrate another successful synthesis of Cr_2O_3 using cubic mesoporous silica KIT-6. It is of great interest to find that the crystal orientation of Cr_2O_3 has a close relation with the symmetry of the mesopore system in KIT-6. Since the crystals formed in nanoscale channels, we believe that it is worth paying attention to a nanoreactor-effect to the crystal growth.

Chromium oxide (Cr_2O_3) plays an important role in magnetics and catalysis,[20,21] and it is believed that its porous single-crystal form may have distinct properties due to its high surface area and patterned nanoscale pores. In the previous studies, we have prepared 3-D porous single-crystals of Cr_2O_3 using γ-aminopropyltriethoxylsilane (APTES) modified SBA-15 mesoporous silica as the template and $H_2Cr_2O_7$ as the precursor.[18] Recently, a "two solvents" impregnation method, derived from incipient wetness impregnation technique, has been adopted to synthesize nanostructured spinel $CoFe_2O_4$ and α-MnO_2,[22,23] and the filling efficiency of the template channels and homogeneity of the products have been improved. With the "two-solvents" method, we prepared mesoporous single-crystals of Cr_2O_3 using chromium nitrate as the precursor and cubic *Ia*3*d* mesoporous KIT-6 silica as the template, which contains 3-D bicontinuous channel networks.[9]†

After chromium nitrate was embedded within the mesopores of KIT-6, the thermal decomposition of the precursor was monitored by variable-temperature *in situ* X-ray diffraction (XRD) in the large-angle region. As shown in Fig. 1, at room temperature the sample exhibits only a hump centred at 24°, attributing to amorphous structure of the silica. The XRD patterns at 373 and 473 K further indicate the high dispersion of chromium nitrate in an amorphous state and, when above the decomposition temperature of the nitrate (*ca.* 100 K), the amorphous state of chromium oxide. A crystalline phase with the diffraction pattern indexed to the rhombohedral phase of Cr_2O_3 (JCPDS No. 01-1294, a = 0.495 nm, c = 1.366 nm, space group $R\bar{3}c$) appears above 473 K and shows no significant changes when the specimen was treated at higher temperature or cooled to room temperature. The XRD pattern of the silica-free Cr_2O_3 sample is also shown in Fig. 1, indicating that the crystalline phase remains unchanged in absence of the amorphous silica after removal of the silica template.

The XRD patterns of both crystalline chromium oxide and KIT-6 in the small-angle region are shown in Fig. 2. The

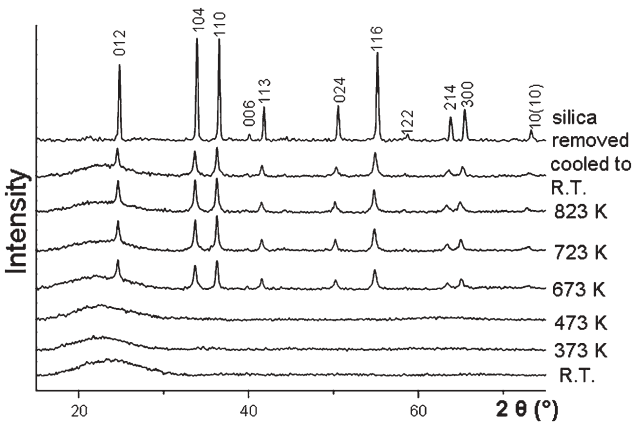

Fig. 1 *In-situ* XRD patterns of $Cr(NO_3)_3$/KIT-6 and silica-free Cr_2O_3 in a temperature range from room temperature to 823 K. The top diffraction is indexed onto the unit cell of rhombohedral Cr_2O_3.

[a]*Department of Chemistry & Shanghai Key Laboratory of Molecular Catalysis and Innovative Materials, Fudan University, Shanghai, 200433, P. R. China. E-mail: heyonghe@fudan.edu.cn*
[b]*School of Chemistry, St. Andrews University, St. Andrews, Fife, UK KY16 9ST. E-mail: wzhou@st-andrews.ac.uk; Fax: (+44) 1223-463808*

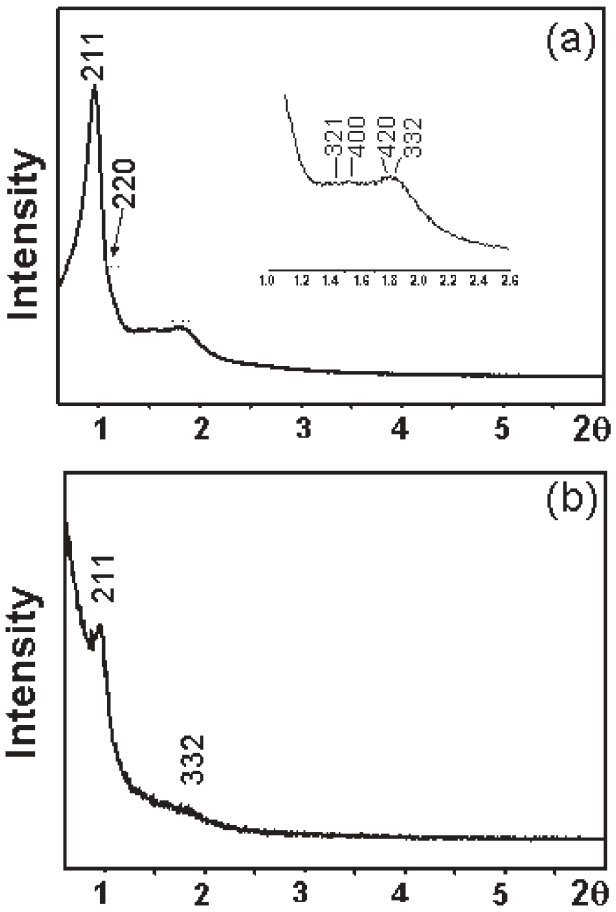

Fig. 2 Small-angle XRD patterns of (a) mesoporous cubic KIT-6 silica, space group *Ia3d* and (b) its negative replica, porous single-crystals of Cr_2O_3.

characteristic diffraction peaks of the cubic structure of the mesoporous Cr_2O_3 can be observed although they are not very well resolved in comparison with those from its template KIT-6. The unit cell parameter of the mesoporous Cr_2O_3 calculated from the (211) diffraction is 22.7 nm, which is almost equal to that of KIT-6 (a = 22.8 nm). Consequently, it can be confirmed that the mesostructure of the Cr_2O_3 product is a negative replica of KIT-6.

The replication of the KIT-6 silica by Cr_2O_3 can also be directly observed in the transmission electron microscopic (TEM) images. Fig. 3(a) shows a typical porous single-crystal of Cr_2O_3 with a diameter of *ca.* 300 nm, which is much smaller than the KIT-6 silica particles, which ranges from several microns to tens of microns. This may be due to mass transfer along different directions and disconnection of Cr_2O_3 crystals during thermal decomposition and crystallization. Another interesting feature, other than the particle size, is that the particles tend to be spherical in shape. This indicates a 3D growth resulted from the 3D pore system in KIT-6, which is different from the morphology of the porous crystals templated by SBA-15. The hexagonal image contrast pattern in Fig. 3(a), where the mesopores are seen as bright contrast, indicates that the image is viewed down the [111] zone axis of the KIT-6 related cubic unit cell and the cell dimension is similar to that of KIT-6, in a good agreement with the small-angle XRD in Fig. 2. The single-crystallinity can be proved by the corresponding SAED pattern from the whole

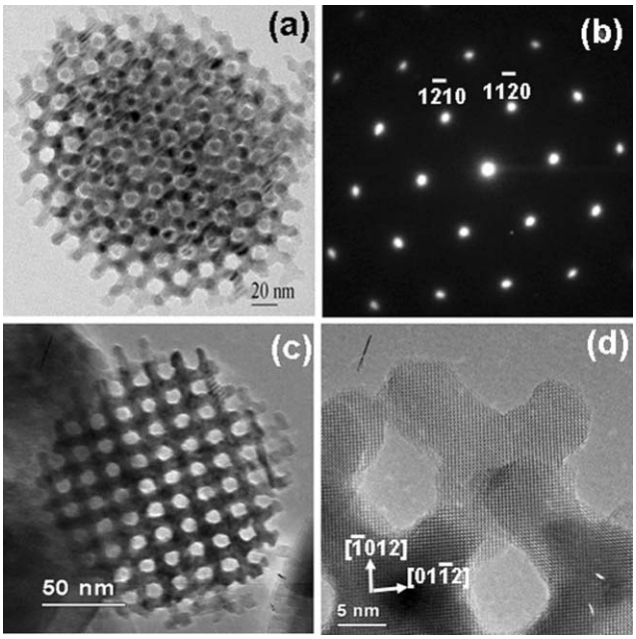

Fig. 3 TEM examination of porous single-crystal of Cr_2O_3 viewed down two principal zone axes. (a) TEM image showing mesopore structure along the [111] direction of the KIT-6 related cubic unit cell and (b) the corresponding SAED pattern indexed onto the rhombohedral unit cell of Cr_2O_3 crystal. (c) TEM image showing the mesopore structure along the [100] zone axis of the KIT-6 related unit cell and (d) corresponding HRTEM image on the $[2\bar{2}1]$ zone axis of Cr_2O_3 unit cell.

particle shown in Fig. 3(b) without specimen tilting. This SAED pattern can be indexed on to the rhombohedral Cr_2O_3 with the view direction of [001]. Consequently, the 6-fold axes in the KIT-6-like cubic mesoporous unit cell (along the [111] axis) and in Cr_2O_3 (along the [001] axis) are perfectly parallel to each other.

Fig. 3(c) is another TEM image of porous crystal of Cr_2O_3 with an even smaller size, viewed down the [100] zone axis of the KIT-6 related cubic mesostructural unit cell. A perfect square pattern of the mesopores can be seen. Fig. 3(d) is the corresponding HRTEM image recorded from a corner of the particle in Fig. 3(c). The two principal d-spacings measured from the image are 0.36 and 0.37 nm, corresponding to the $(\bar{1}02)$ and (012) planes, respectively. The interplane angle is about 94°. It is therefore found that the viewing direction is along the $[2\bar{2}1]$ axis of Cr_2O_3. The atomic image contrast shows the crystal structure to be very close to a square pattern. The angle between the [111] and [100] zone axes in the cubic KIT-6 structure is 54.7°, while that between the [001] and $[2\bar{2}1]$ zone axes in the rhombohedral Cr_2O_3 structure is 51.5°. Consequently, we assume the two particles presented in Fig. 3 have the same crystal orientation related to the KIT-6 pore system and the orientation of the porous crystal of Cr_2O_3 seems to have a close relation with the structural symmetry of KIT-6.

Fig. 4 shows the nitrogen adsorption–desorption isotherms of KIT-6, Cr_2O_3/KIT-6 and silica-free mesoporous single-crystal Cr_2O_3. The isotherms of KIT-6 and Cr_2O_3/KIT-6 are of type IV classification, which have typical hysteresis loops of mesoporous materials. The parent KIT-6 has a surface area of 453 $m^2\ g^{-1}$, a pore volume of 0.71 $cm^3\ g^{-1}$ and a pore size of 6.1 nm, while the Cr_2O_3/KIT-6 has a smaller surface area and pore volume of 347 $m^2\ g^{-1}$ and 0.54 $cm^3\ g^{-1}$, respectively, but the pore size

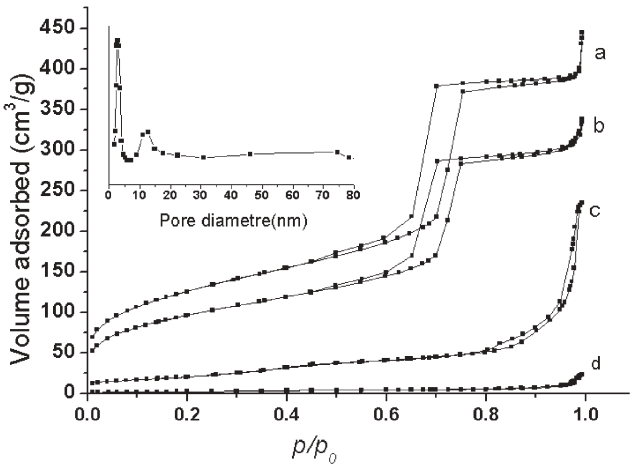

Fig. 4 Nitrogen adsorption–desorption isotherms at 77 K of (a) mesoporous silica KIT-6, (b) mesostructured Cr_2O_3/KIT-6 composite, (c) silica-free mesoporous Cr_2O_3, and (d) bulk Cr_2O_3. The inset is the pore size distribution of silica-free mesoporous Cr_2O_3.

(6.1 nm) is maintained. This indicates that the part of KIT-6 pores become empty after the formation of Cr_2O_3 from chromium nitrate. The silica-free mesoporous single-crystal Cr_2O_3 sample has a surface area of 86 m^2 g^{-1} and a pore volume of 0.61 cm^3 g^{-1}, which are much larger than those for bulk Cr_2O_3. It is noticeable that its isotherm is different from that of KIT-6 and Cr_2O_3/KIT-6, giving wide pore size distributions centred at 3.1 and 12.3 nm, indicating expected irregular pore shapes. The former reflects the minimum wall thickness of KIT-6 [9] whereas the latter is corresponding to the wall junctions in KIT-6, or to the pore size observed from the TEM images (Fig. 3).

In contrast, the shape of the Cr_2O_3 nanowires, which are the building units for the mesoporous network, is quite regular, reflecting the shape of the mesopores in KIT-6. Directly observed from the TEM images, we can see that these nanowires have round cross section and uniform diameter of about 6 nm, which is close to the value of mesopores in KIT-6 detected by the adsorption-desorption method. The specific locations of the mesopores in KIT-6 have also been replicated by the Cr_2O_3 nanowires. Consequently, the mesopore system in KIT-6 has been fully replicated by single-crystals of Cr_2O_3.

Although little has been done to understand why the orientation of the Cr_2O_3 crystals is closely related to the symmetry of the KIT-6 mesopore system, this novel phenomenon implies that, when the container (mesopores in the present case) for crystal growth reduces to a nanometer scale, its thermoresonance may have a significant inference on the crystal growth, leading to a certain crystal orientation which allows the highest density of the product in the limited space of the container.

In summary, the present work demonstrates the successful growth of porous single-crystal Cr_2O_3 with a unique 3-D mesopore system using cubic mesoporous silica KIT-6 as a template. The products are believed to be mechanically much stronger than amorphous or polycrystalline Cr_2O_3 mesoporous materials. Based on our studies, this method may be used to develop other oxides and mixed oxides with the same porous system. Those materials have potential to be used as self-supported catalysts with a high activity due to their large surface area and shape selectivity. Further investigation on the formation mechanism, the effect of nanoreactor on the crystal orientation, physico-chemical properties of these porous single-crystals will be carried out in these laboratories.

This work was supported by the National Science Foundation of China (20371013, 20273017, 20025310, 20421303), National Basic Research Program of China (2003CB615807) and Shanghai Science and Technology Committee (03DJ14004). W. Z. thanks EPSRC for the studentship for C. D.

Notes and references

† Mesoporous silica KIT-6 was prepared according to the reported procedure.[9] The Cr_2O_3 loaded samples were prepared by suspending 1.0 g KIT-6 in dry *n*-hexane, used as the first solvent. After stirring for 3 h, 1.0 ml aqueous solution (8.0 g $Cr(NO_3)_3 \cdot 9H_2O$ in 3.7 g H_2O) as the second solution was added dropwise with vigorous stirring. The mixture was stirred overnight and then a powder specimen was obtained by filtration and drying at 40 °C. The solid was then calcined in a muffle furnace with a heating rate of 1 °C min^{-1} from room temperature to 550 °C and then maintained at 550 °C for 5 h. The mesoporous Cr_2O_3 single-crystals were finally obtained by the removal of silica with 10% HF. Small-angle and normal XRD measurements were performed on a Rigaku D/MAX-IIA X-ray diffractometer using Cu-Kα radiation. TEM was performed using a JOEL JEM-2010 electron microscope. Nitrogen adsorption–desorption measurements were performed on a Micromeritics Tristar 3000 system at 77 K.

1 Z. S. Chao and E. Ruchenstein, *Langmuir*, 2002, **18**, 734.
2 D. M. Antonelli and J. Y. Ying, *Angew. Chem., Int. Ed. Engl.*, 1996, **35**, 426.
3 P. D. Yang, D. Y. Zhao, D. I. Margolese, B. F. Chmelka and G. D. Stucky, *Nature*, 1998, **396**, 152.
4 B. Z. Tian, X. Y. Liu, B. Tu, C. Z. Yu, J. Fan, L. M. Wang, S. H. Xie, G. D. Stucky and D. Y. Zhao, *Nat. Mater.*, 2003, **2**, 159.
5 D. Grosso, C. Boissière, B. Smarsly, T. Brezesinski, N. Pinna, P. A. Albouy, H. Amenitsch, M. Antonietti and C. Sanchez, *Nat. Mater.*, 2004, **3**, 787.
6 J. S. Beck, J. C. Vartuli, W. J. Roth, M. E. Leonowicz, C. T. Kresge, K. D. Schmitt, C. T. W. Chu, D. H. Olson, E. W. Sheppard, S. B. McCullen, J. B. Higgins and J. L. Schlenker, *J. Am. Chem. Soc.*, 1992, **114**, 10834.
7 D. Y. Zhao, J. Feng, Q. Huo, N. Melosh, G. H. Fredrickson, B. F. Chmelka and G. D. Stucky, *Science*, 1998, **279**, 548.
8 D. Y. Zhao, Q. S. Huo, J. L. Feng, B. F. Chmelka and G. D. Stucky, *J. Am. Chem. Soc.*, 1998, **120**, 6024.
9 F. Kleitz, S. H. Choi and R. Ryoo, *Chem. Commun.*, 2003, 2136.
10 U. Ciesla, D. Demuth, R. Leon, P. Petroff, G. Stucky, K. Unger and F. Schüth, *J. Chem. Soc., Chem. Commun.*, 1994, 1387.
11 S. Ayyappan, N. Ulagappan and C. N. R. Rao, *J. Mater. Chem.*, 1996, **6**, 1737.
12 D. S. Xu, Y. J. Xu, D. P. Chen, G. L. Guo, L. L. Gui and Y. Q. Tang, *Chem. Phys. Lett.*, 2000, **325**, 340.
13 B. Z. Tian, X. Y. Liu, H. F. Yang, S. H. Xie, C. Z. Yu, B. Tu and D. Y. Zhao, *Adv. Mater.*, 2003, **15**, 1370.
14 K. Matsui, B. K. Pradhan, T. Kyotani and A. Tomita, *J. Phys. Chem. B*, 2001, **105**, 5682.
15 H. J. Shin, C. H. Ko and R. Ryoo, *J. Mater. Chem.*, 2001, **11**, 260.
16 H. J. Shin, R. Ryoo, Z. Liu and O. Terasaki, *J. Am. Chem. Soc.*, 2001, **123**, 1246.
17 Y. Q. Wang, C. M. Yang, W. Schmidt, B. Spliethoff, E. Bill and F. Schüth, *Adv. Mater.*, 2005, **17**, 53.
18 K. K. Zhu, B. Yue, W. Z. Zhou and H. Y. He, *Chem. Commun.*, 2003, 98.
19 B. Yue, H. Tang, Z. Kong, K. Zhu, C. Dickinson, W. Z. Zhou and H. He, *Chem. Phys. Lett.*, 2005, **407**, 83.
20 N. R. Jana, Y. F. Chen and X. G. Peng, *Chem. Mater.*, 2004, **16**, 3931.
21 T. Yokoyama and N. Fujita, *Appl. Catal., A*, 2004, **276**, 179.
22 C. Pham-Huu, N. Keller, C. Estournès, G. Ehret and M. J. Ledoux, *Chem. Commun.*, 2002, 1882.
23 M. Imperor-Clerc, D. Bazin, M. Appay, P. Beaunier and A. Davidson, *Chem. Mater.*, 2004, **16**, 1813.

